Acta Pharmacologica Sinica

www.nature.com/aps

ARTICLE

# Skullcapflavone II, a novel NQO1 inhibitor, alleviates aristolochic acid I-induced liver and kidney injury in mice

Ya-ping Dong[1], Shu-zhen Chen[2,3], Hui-si He[2,3], Zhuo-ran Sun[4], Li-xuan Jiang[2,3], Yan-qiu Gu[5], Ying Zhang[4], Fei Feng[4], Chun Chen[6], Zhe-cai Fan[2,3], Xiao-fei Chen[4], Wen Wen[2,3] and Hong-yang Wang[1,2,3,7]

Aristolochic acid I (AAI) is a well established nephrotoxin and human carcinogen. Cytosolic NAD(P)H quinone oxidoreductase 1 (NQO1) plays an important role in the nitro reduction of aristolochic acids, leading to production of aristoloactam and AA-DNA adduct. Application of a potent NQO1 inhibitor dicoumarol is limited by its life-threatening side effect as an anticoagulant and the subsequent hemorrhagic complications. As traditional medicines containing AAI remain available in the market, novel NQO1 inhibitors are urgently needed to attenuate the toxicity of AAI exposure. In this study, we employed comprehensive 2D NQO1 biochromatography to screen candidate compounds that could bind with NQO1 protein. Four compounds, i.e., skullcapflavone II (SFII), oroxylin A, wogonin and tectochrysin were screened out from *Scutellaria baicalensis*. Among them, SFII was the most promising NQO1 inhibitor with a binding affinity ($K_D = 4.198$ μmol/L) and inhibitory activity ($IC_{50} = 2.87$ μmol/L). In human normal liver cell line (L02) and human renal proximal tubular epithelial cell line (HK-2), SFII significantly alleviated AAI-induced DNA damage and apoptosis. In adult mice, oral administration of SFII dose-dependently ameliorated AAI-induced renal fibrosis and dysfunction. In infant mice, oral administration of SFII suppressed AAI-induced hepatocellular carcinoma initiation. Moreover, administration of SFII did not affect the coagulation function in short term in adult mice. In conclusion, SFII has been identified as a novel NQO1 inhibitor that might impede the risk of AAI to kidney and liver without obvious side effect.

**Keywords:** aristolochic acids; skullcapflavone II; NAD(P)H quinone oxidoreductase 1 (NQO1); hepatorenal toxicity; DNA damage; dicoumarol

*Acta Pharmacologica Sinica* (2023) 44:1429–1441; https://doi.org/10.1038/s41401-023-01052-3

## INTRODUCTION

Aristolochic acids (AAs) are a class of naturally produced nitrophenanthrene carboxylic acids, which are widely found in medicinal herbs of the Aristolochiaceae family, such as *Aristolochiae fructus* and *Asarum* [1]. The extracts from Aristolochiaceae herbs were previously investigated, resulting in the discovery of 4 main components, including aristolochic acid I, II, III, and IV [2], with aristolochic acid I (AAI) being the predominant toxic compound [3]. AAs have been shown to cause renal damage [4, 5], recognized as aristolochic acid nephropathy (AAN). Moreover, our previous study found that AAI could also induce the development of spontaneous liver cancer when given to infant mice [6]. Since considerable attention has been drawn to the safe use of AAs in China, the use of some herbs of the genus *Aristolochia* and *Asarum* has been prohibited. However, in 2017, the China Food and Drug Administration announced that there were still 43 kinds of Chinese patent medicine containing *Aristolochia* available in the market.

Aristoloactam (AL), the product of aristolochic acid metabolism, can react with DNA to form DNA adduct (AA-DNA adduct), subsequently induces A to T transversion mutation, and finally DNA damage [7]. The metabolism of AAs is a complicated process involving a series of catalyzed chemical reactions and a variety of key enzymes. NAD(P)H quinone oxidoreductase 1 (NQO1) plays an important role in the nitro reduction of AAs, resulting in the production of AL and AA-DNA adduct [8]. NQO1 can catalyze the reduction of quinones, nitroaromatic compounds, and azoxy compounds, reducing a wide range of quinones to hydroquinone [9, 10]. Currently, dicoumarol is the most widely used and effective NQO1 inhibitor. However, it is also a long-acting anticoagulant [11]. The anticoagulant effects and the subsequent hemorrhagic complications greatly limited the clinical use of dicoumarol [12]. Consequently, a novel NQO1 inhibitor is urgently needed to alleviate AAs-related toxicity without severe side effects.

A well-known Chinese herb, *Scutellaria baicalensis*, has been utilized extensively in traditional Chinese medicine and has

[1]Fudan University Shanghai Cancer Center, Department of Oncology, Shanghai Medical College, Fudan University, Shanghai 200032, China; [2]National Center for Liver Cancer, Naval Medical University (Second Military Medical University), Shanghai 200438, China; [3]International Cooperation Laboratory on Signal Transduction, Eastern Hepatobiliary Surgery Hospital, Naval Medical University (Second Military Medical University), Shanghai 200438, China; [4]School of Pharmacy, Naval Medical University (Second Military Medical University), Shanghai 200433, China; [5]Department of Pharmacy, Shanghai Ninth People's Hospital, Shanghai Jiao Tong University School of Medicine, Shanghai 200011, China; [6]Shanghai Jiao Tong University School of Medicine, Shanghai 200025, China and [7]State Key Laboratory of Oncogenes and Related Genes, Shanghai Cancer Institute, Renji Hospital, Shanghai Jiao Tong University School of Medicine, Shanghai 200032, China
Correspondence: Xiao-fei Chen (xfchen2010@163.com) or Wen Wen (wenwen_smmu@163.com) or Hong-yang Wang (hywangk@vip.sina.com)
These authors contributed equally: Ya-ping Dong, Shu-zhen Chen, Hui-si He.

Received: 19 August 2022 Accepted: 8 January 2023
Published online: 25 January 2023

demonstrated a wide spectrum of pharmacological activities, including bacteriostatic, anti-inflammatory, anti-oxidant, and anti-tumor effects [13, 14]. *Scutellaria baicalensis* is rich in various active flavonoids [15], which has a similar structure to dicoumarol. Pharmacological researchers have found that the active ingredients of *Scutellaria baicalensis* could attenuate the liver and kidney injury induced by a variety of toxic substance [16–19]. Due to the complex ingredients of traditional Chinese medicine, it is a great challenge to further identify the effective components. Biochromatography is a biological affinity chromatography technique that uses a protein as a stationary phase for chromatographic separation and characterization of sample components [20, 21]. Therefore, a comprehensive two-dimensional (2D) NQO1 biochromatography system was employed to screen bioactive components from *Scutellaria baicalensis* to analyze the interaction between its components and NQO1 protein.

Hence, four active candidate components were screened from the extract of *Scutellaria baicalensis* by the above system. Subsequently, using the surface plasmon resonance (SPR) analysis and NQO1 inhibitory activity assay, we identified a novel NQO1 inhibitor with desirable affinity and inhibitory activity, skullcapflavone II (SFII). In this study, we aimed to explore the potentiality and the underlying mechanisms of SFII in alleviating AAI-induced hepatorenal toxicity as a novel NQO1 inhibitor. Generally, this study may provide a new clue for the application of SFII in the detoxification of AAs-induced damage.

## MATERIALS AND METHODS

### Chemical and reagent

Human NQO1 recombinant protein was obtained from Synpeptide Co., Ltd. (Nanjing, China). Aristolochic acid I (AAI, A5512), mercaptopropyltrimethoxysilane (MPTS), *N*,*N*-Dimethylformamide (DMF), and N-(4-maleimide butyryloxide) succinimide (GMBS) were obtained from Sigma (St. Louis, MO, USA). Silica gel was obtained from Qingdao Meigao Chemical Co., Ltd. (Qingdao, China). Skullcapflavone II (SFII) was bought from Shanghai Huizhou Bio-Technology Co., Ltd. (HZ-HQXI98-50, Shanghai, China). Dicoumarol was obtained from Selleck Chemicals (S4299, Houston, TX, USA). Oroxylin A (B20958), wogonin (B20489), and tectochrysin (B21459) were purchased from Shanghai Yuanye Bio-Technology Co., Ltd. (Shanghai, China). Dimethyl sulfoxide (DMSO) was purchased from WAK-Chemie (WAK-DMSO-70, Berlin, Germany). $CCl_4$, olive oil, and $NaHCO_3$ were bought from Sinopharm Chemical Reagent Co., Ltd. (Shanghai, China).

### Preparation of NQO1 biochromatographic stationary phase

The synthesis of the NQO1 biochromatographic stationary phase was done according to the published research method [21] and was shown in the second step of Fig. 1. Synthesis process: 1 g silica gel (5 μm, 200 Å) and 1 mL MPTS were added in 100 mL DMF, and the solution system was stirred under the conditions of nitrogen protection and 60 °C for 5 h. Then, the suspension obtained from the reaction was centrifuged at 5000× *g* and washed with DMF 3 times. Subsequently, the obtained precipitate was stirred in 5% GMBS (dissolved in 500 mL DMSO) at room temperature for 2 h. DMSO was used to wash the MPTS/GMBS-modified silica gel for 3 times and the gel was dried in a vacuum for 48 h. Under the condition of 4 °C, 20 μg of human NQO1 recombinant protein and 40 mg MPTS/GMBS-modified silica gel were stirred in phosphate buffer solution (PBS) for 12 h, and the NQO1 recombinant protein could be immobilized in the stationary phase. The NQO1 Activity Assay Kit (ab184867, Abcam, Cambridge, MA, USA) was used to determine the biological activity of the chromatographic stationary phase, and the color development and rate (mOD/min) per sample well were recorded.

### Comprehensive 2D NQO1 biochromatography system

The comprehensive 2D NQO1 biochromatography system was aboard on an Agilent 1200 series high-performance liquid chromatography system combined with time-of-flight mass spectrometer (TOFMS), controlled by Agilent MassHunter Workstation (Agilent Technologies, Palo Alto, CA, USA). With ammonia acetate as the mobile phase, the NQO1 column was used as the first-dimensional column. Besides, an Agilent Poroshell 120 EC-C18 column was used as the second dimension, with acetonitrile and 0.1% formic acid as the mobile phase. The relevant operating details of the comprehensive 2D NQO1 column/C18 column/TOFMS system could be referred to in the literature [22, 23]. The system was equilibrated for 30 min, and 3 μL of the *Scutellaria baicalensis* extract was injected into the system. In order to obtain the comprehensive 2D NQO1 biochromatographic analysis results, system collects at least two fractions across a retention peak. Therefore, the collection period of each round was set to 2.5 min. Subsequently, the machine collected the information on the stable retention behavior and molecular structure of components in extract of *Scutellaria baicalensis*. Relevant data were analyzed for baseline correction and 2D mapping of retention behavior.

### NQO1 enzyme activity test

The inhibition activities of candidate compounds on human NQO1 recombinant protein, cell and mouse samples were detected by the NQO1 Activity Assay Kit (ab184867, Abcam, Cambridge, MA, USA). The sample and reaction buffer were added to 96 well plates, and the absorbance at 440 nm was recorded by a microplate reader. GraphPad Prism 8.0.1 (LaJolla, CA, USA) was used to calculate the 50% inhibiting concentration ($IC_{50}$) and fit the inhibition curve.

### Surface plasmon resonance (SPR) analysis

The Biacore T200 system (GE Healthcare Life Sciences, Marlborough, MA, USA) was used for SPR assays. The acetic acid buffer (pH = 4.0) was used to dilute NQO1 recombinant protein (His tag), and the protein was covalently immobilized in Series S Sensor Chip CM5 (BR100530, GE Healthcare Life Sciences, Marlborough, MA, USA). The candidate compounds were subjected to gradient dilution with PBS buffer containing 5% DMSO and then injected into the NQO1 recombinant protein channel and the control channel, and the flow rate of the running buffer was set to 30 mL/min. The coupling time was 60 s and the dissociation time was 300 s. The Biacore T200 was used to analyze the experimental data, calculate the equilibrium dissociation constant ($K_D$), and fit the affinity curve.

### Molecular docking

The structure of NQO1 protein was obtained from the Protein Data Bank (PDB ID: 1D4A). The molecular structures of candidate compounds were downloaded from PubChem. Schrö-dinger v2019. 03 (Schrödinger Inc., Plainview, NY, USA) software was used to simulate the candidate molecular docking to NQO1 protein, and to predict the binding sites of the candidate molecule and NQO1 protein.

### Animal experiment

C57BL/6 mice were purchased from the Model Animal Resource Information Platform (Nanjing, China). All animal experiments were performed following the NIH guidelines and approved by the Ethics Committee of the Shanghai Cancer Center, Fudan University. Ethical Approval Number: FUSCC-IACUC-S2022-0114.

For the C57BL/6 adult mice (male) acute renal injury model, animals were given indicated doses of AAI or SFII at the age of 8 weeks. Mice were divided into four groups: $NaHCO_3$ group, AAI (5 mg/kg) group, and SFII (30 or 60 mg/kg) + AAI (5 mg/kg) group. Mice were sacrificed 3 days after the first dose of AAI administration.

For the adult mice (male) renal fibrosis model, animals were divided into four groups: $NaHCO_3$ group, AAI (10 mg/kg) group, and SFII (30 or 60 mg/kg) + AAI (10 mg/kg) group. The AAI group was pretreated with olive oil 12 h by gavage in advance, followed by a single intraperitoneally (*i.p.*) injection of AAI and subsequent (olive oil) for 3 days. SFII and AAI combined treatment groups were pretreated with SFII (30 or 60 mg/kg) by gavage 12 h in advance, followed by a single *i.p.* injection of AAI and subsequent SFII by gavage for 3 days. Mice were sacrificed 14 days after the first dose of AAI.

For the infant mice acute injury model, male mice were given indicated doses of AAI or SFII at the age of 14 days. Infant mice were divided into the following groups: $NaHCO_3$ group, AAI group, and SFII (10 mg/kg) + AAI group. Mice were sacrificed 24 h after AAI administration. For the AAI-induced liver cancer model, a single injection of AAI or $NaHCO_3$ was given to male infant mice on the 14th day after birth. Mice (6 mice/group) were divided into five groups: $NaHCO_3$ group, AAI (20 mg/kg) group, and the SFII (10, 30, or 60 mg/kg) + AAI (20 mg/kg) group. For each group, mice were sacrificed 16 weeks after a single dose of $NaHCO_3$ or AAI.

Additional details of the animal models are available in Supplementary Materials.

### Blood coagulation assay

Mice (4 mice/group) were administered with dicoumarol, oroxylin A and SFII orally at dose of 6 mg/kg respectively and then sacrificed after 24 h. Blood samples of mice were taken to detect the activated partial thromboplastin time (APTT), prothrombin time (PT), and thrombin time (TT). The coagulation test reagents of APTT, PT, and TT were purchased from Siemens (Berlin, Germany). The Sysmex CS-5100 (Kobe, Japan) was used for coagulation assays of blood samples.

### Cell culture

Human normal liver cell line (L02) and human renal proximal tubular epithelial cell line (HK-2) were obtained from the Cell Bank of the Chinese Academy of Sciences (Shanghai, China). L02 was cultured with DMEM medium (Gibco, Grand Island, NY, USA), which was supplemented with 1% antibiotic-antimycotic solution and 10% fetal bovine serum (FBS, Biological Industries, Kibbutz Beit Haemek, Israel). HK-2 was cultured with Dulbecco's modified Eagle's medium/Nutrient Mixture F-12 (DMEM/F12, Gibco, Grand Island, NY, USA), which contained 1% antibiotic-antimycotic solution and 10% FBS (Gibco, Grand Island, NY, USA). All cells were cultured in a humidified incubator containing 5% carbon dioxide at 37 °C.

### Construction of NQO1 knockdown cell line

Recombinant lentivirus vectors containing the interference NQO1 plasmid (shNQO1) and negative control (shNC) were purchased from Shanghai Genechem (Shanghai, China). L02 with 50% density in a 6-well plate was infected by a concentrated virus (200 μL) with polybrene for 10 h. Lentivirus infected L02 cells were treated with puromycin (2 μg/mL) for 48 h. The knockdown effect of NQO1 in infected cells was verified by quantitative real-time PCR (qRT-PCR) and Western blot.

### Cell proliferation assay

The cells were inoculated into 96 well plates and cultured overnight in a 5% $CO_2$ incubator at 37 °C. AAI (dissolved in 1% $NaHCO_3$) and SFII (dissolved in DMSO) were added to the culture medium. At the time points of 0 h, 24 h, and 48 h, the culture medium in the well was replaced with a CCK-8 reagent (CK04, Dojindo, Kumamoto, Japan), and the plates were placed in the 37 °C incubators for 2 h. Subsequently, the absorbance per well was measured at 450 nm by a microplate reader.

### Western blot

Cell lysis buffer for Western blot (P0013, Beyotime, Shanghai, China) was added to the cells and tissues of mice to extract the whole protein. The protein concentration was determined by BCA Protein Assay Kit (23227, Invitrogen, Carlsbad, CA, USA). The SDS-PAGE gel (PG113, Epizyme, Shanghai, China) was used for electrophoresis, and then the proteins were transferred to the nitrocellulose (NC) blotting membrane. The NC membranes were incubated with primary antibodies which included P53 (SC-126, Santa Cruz, CA, USA), NQO1 (3187S, CST, Danvers, MA, USA), β-Actin (AC004, Abclonal, Wuhan, China), GAPDH (AC033, Abclonal, Wuhan, China), γ-H2AX (ab11174, Abcam, Cambridge, MA, USA), cleaved caspase-3 (9664T, CST, Danvers, MA, USA) and PARP-1 (9532T, CST, Danvers, MA, USA). The membranes were scanned by an Odyssey CLx image scanner system (Li-COR, Lincoln, NE, USA).

### Flow cytometry analysis

The cells were inoculated in a 6-well plate and cultured overnight in a 5% $CO_2$ incubator at 37 °C. AAI and SFII were added to the culture medium for 24 h. The cells were digested with trypsin, centrifuged at 1000 rpm for 3 min, and washed with PBS. Then, 5 μL Annexin V-FITC reagent (C1062L, Beyotime, Shanghai, China) or Annexin V-APC reagent (550474, BD Pharmingen, San Diego, CA, USA), 10 μL PI reagent, and 195 μL binding solution was added to per sample tube. Cells and reagents were incubated at room temperature in the dark for 20 min, and then BD FACSCelesta (BD, Franklin Lakes, NJ, USA) was used for flow cytometry analysis.

### The quantitative real-time PCR (qRT-PCR) assay

Total RNA was extracted from cells using Trizol (Invitrogen, Carlsbad, CA, USA). The cDNA was synthesized using a reverse transcription system which included M-MLV reverse transcriptase (M1701, Promega, Madison, USA), Ribonuclease Inhibitor (N2515, Promega, Madison, USA), dNTP, and N6 randomized primer. Subsequently, SYBR® Green Master (4913914001, Roche, Basel, Switzerland) based, the indicated gene was amplified with cDNA as the template by specific primers through LightCycler (Roche, Basel, Switzerland). The primer sequences were listed in Supplementary Table S1.

### Sirius red staining

The sections of tissues were dewaxed in xylene and rehydrated in gradient alcohol. Sirius red dye (9046, Chondrex, Redmond, WA, USA) was added to the sections and incubated in 37 °C incubator for 30 min. The sections were washed in $ddH_2O$, and then dehydrated in 100% ethanol for 5 min. Subsequently, the sections were soaked in xylene for 5 min, and mounted in a resinous medium.

### TUNEL staining

We detected the apoptosis of mouse tissues with the Biotin TUNEL Assay Apoptosis Detection Kit (T6068, US EVERBRIGHT INC, Suzhou, China). The sections of tissues were dewaxed in xylene and rehydrated in gradient alcohol. Protein K was added to the sections and incubated at room temperature for 20 min. The sections were exposed to 100 μL of 0.3% $H_2O_2$ solution and incubated at room temperature for 30 min to inactivate the endogenous peroxidases. The TUNEL reaction solution (50 μL) was added to sections and incubated at 37 °C incubators in the dark for 2 h. Subsequently, the sections were exposed to 50 μL Streptavidin-HRP solution and incubated at 37 °C incubators in the dark for 30 min. Finally, DAB (K3468, Dako, Glostrup, Denmark) was used for the chromogenic reaction of sections.

### H&E (hematoxylin-eosin) staining

The tissues were fixed in 10% formaldehyde solution for 24 h, and dehydrated by Leica ASP300S (Leica, Wetzlar, Germany). The tissues were embedded in paraffin, and cut into 3 μm section. H&E staining was performed on sections using the Leica Autostainer XL (Leica, Wetzlar, Germany Germany), according to the Leica staining protocol.

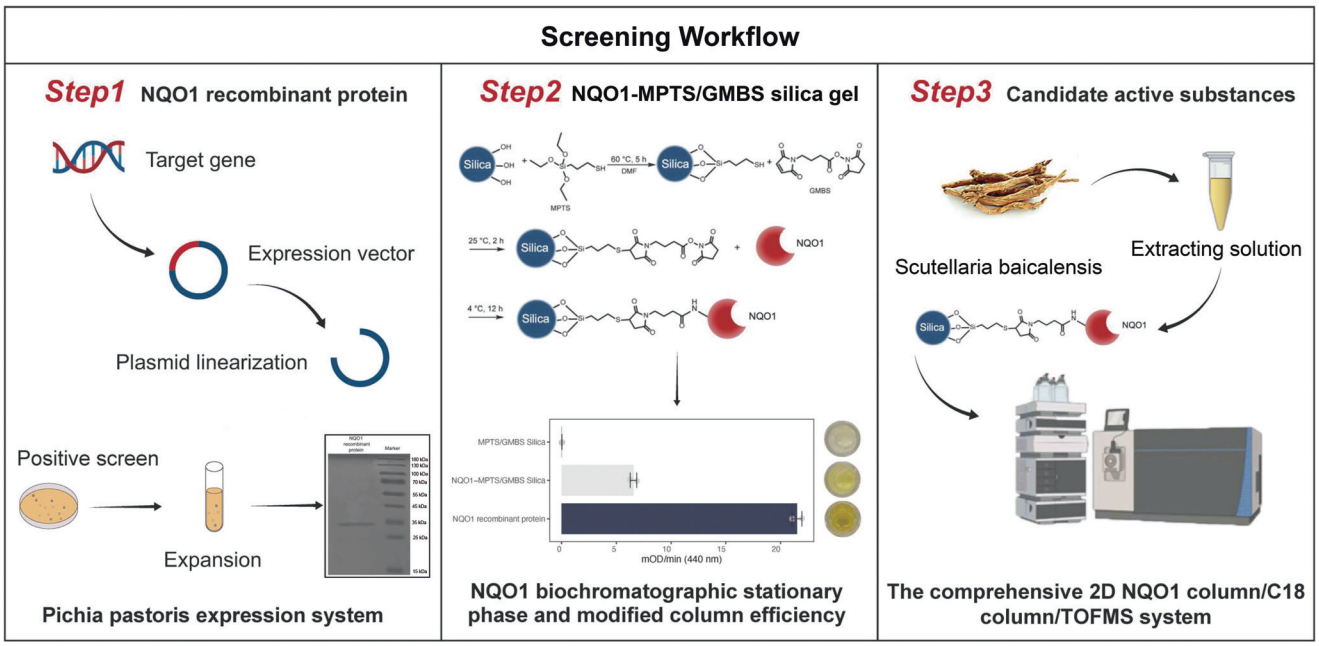


**Fig. 1** Synthetic route of NQO1 biochromatographic stationary phase and screen workflow of NQO1 binding candidate components from the extract of *Scutellaria baicalensis*.

Immunohistochemistry (IHC)

For IHC, the sections of tissues were incubated with the primary antibody at 4 °C overnight, such as the anti-alpha 1 fetoprotein antibody (AFP, 1:500, 009P, Celplor, NC, USA) and anti-Ki-67 antibody (1:300, ab15580, Abcam, Cambridge, MA, USA). Subsequently, the sections were incubated with Supervision$^{TM}$ anti-Rabbit-HRP (D-3002, Longislandbio, Shanghai, China) at 37 °C for 30 min. The DAB (K3468, Dako, Glostrup, Denmark) was used for the chromogenic reaction of section.

Biochemical parameter

The culture medium of L02 was collected to detect the cell damage by Alanine Aminotransferase Test Kit (ALT, Mindray Biomedical, Shenzhen, China) and Aspartate Aminotransferase Test Kit (AST, Mindray Biomedical, Shenzhen, China). The renal function of mice was detected by Creatinine Test Kit (CRE, Mindray Biomedical, Shenzhen, China) and Urea Test Kit (UREA, Mindray Biomedical, Shenzhen, China). The mice were sacrificed at the defined time point, and the serum was separated at the speed of 3000 rpm for 10 min. All biochemical tests were carried out with the full-automatic biochemical analyzer (BS-200, Mindray Biomedical, Shenzhen, China).

Statistical analysis

The GraphPad Prism 8.0.1 (LaJolla, CA, USA) was used for data analysis. Values were expressed as mean ± Standard Deviation (SD). When the data satisfied the normality and homogeneity of variance, the data were statistically analyzed by T-test. The *P*-value tests were two sides in which less than 0.05 were represented as statistically significant.

## RESULTS

Screening of NQO1 binding candidates from the extract of *Scutellaria baicalensis*

To search for the pharmacological agents for attenuating AAs-related toxicity, we employed a biochromatography system [21] to screen and identify candidate compounds that can bind with NQO1 protein (Fig. 1). The purified human NQO1 recombinant protein, with a molecular weight of approximately 35 kDa on SDS-PAGE, was purchased from biosynthesis company. Next, we connected human NQO1 recombinant protein with MPTS/GMBS-modified silica gel to construct a biochromatographic stationary phase. NQO1 protein was covalently bound to the biochromatographic stationary phase retaining good enzyme activity. The final step was to screen potential NQO1 target components from the extract of *Scutellaria baicalensis* by the comprehensive 2D NQO1 column/C18 column/TOFMS system. Dicoumarol, a commonly used NQO1 inhibitor, showed obvious retention on NQO1 biochromatography (Supplementary Fig. S1a). As expected, the negative control, dexamethasone, had no retention on NQO1 biochromatography (Supplementary Fig. S1b). These results indicated that the screening model was highly specific. Four candidate components with retention behaviors were initially identified from this system, including oroxylin A (Fig. 2a), wogonin (Fig. 2a), tectochrysin (Fig. 2b), and SFII (Fig. 2c).

High-efficiency NQO1 inhibitor was identified from active candidates

We then used the NQO1 Activity Assay Kit to detect the inhibitory effects of these four candidate compounds on the enzyme activity of purified NQO1 recombinant proteins. The NQO1 inhibitory activities of dicoumarol and the above four active candidate compounds were expressed as $IC_{50}$ values, which revealed that dicoumarol had strong inhibitory activity, with $IC_{50}$ being 0.09 μmol/L (Supplementary Fig. S1c). As shown in Fig. 2d and Fig. 2e, oroxylin A and SFII showed excellent inhibitory effects on purified NQO1 recombinant proteins, with $IC_{50}$ being 0.93 μmol/L and 2.87 μmol/L, respectively. Wogonin displayed modest NQO1 inhibitory activity, with $IC_{50}$ being 10.15 μmol/L (Fig. 2f), while tectochrysin exhibited the lowest inhibitory efficacy among the 4 compounds, with $IC_{50}$ being 231.50 μmol/L (Fig. 2g). Based on the results of the NQO1 activity inhibitory assay, oroxylin A and SFII were further examined due to excellent inhibitory efficiency.

SPR technology is a gold standard for characterizing drug-target interactions and can provide high-quality kinetic and affinity data [24]. Dicoumarol exhibited a strong binding affinity to NQO1 recombinant protein on SPR ($K_D$ [equilibrium dissociation constant] = 0.162 μmol/L; Supplementary Fig. S1d, e). The $K_D$ values and sensorgrams of oroxylin A and SFII were displayed in Fig. 2h, i,

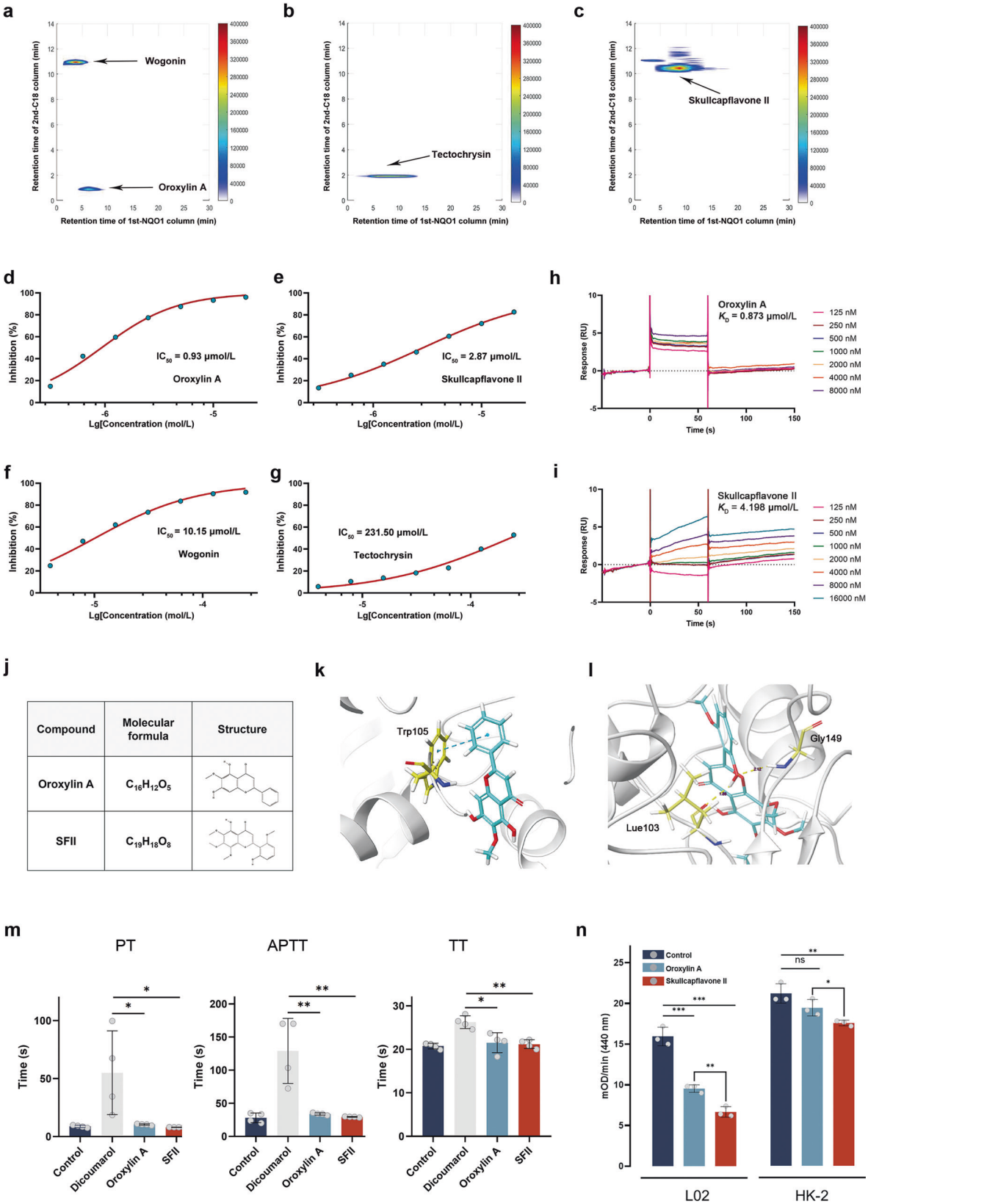


**Fig. 2 The pharmacology analysis of active candidate components.** 2D contour plots of **a** oroxylin A, **a** wogonin, **b** tectochrysin, and **c** SFII were obtained by the comprehensive 2D NQO1 bichromatography system. The inhibitory effects of **d** oroxylin A, **e** SFII, **f** wogonin, and **g** tectochrysin on enzymatic activity of human NQO1 recombinant protein. SPR sensorgrams and $K_D$ of **h** oroxylin A and **i** SFII. **j** The molecular structure of oroxylin A and SFII. Molecular docking results of **k** oroxylin A and **l** SFII with NQO1 protein. **m** Effects of oroxylin A and SFII on APTT, PT, and TT in mice ($n = 4$). **n** The inhibitory effects of oroxylin A and SFII on NQO1 activity in L02 and HK-2 cells. $^*P < 0.05$, $^{**}P < 0.01$, $^{***}P < 0.001$.

in which the $K_D$ values of oroxylin A and SFII were 0.873 μmol/L and 4.198 μmol/L, respectively. The detailed SPR assay results and $K_D$ fitting curves of all compounds were shown in Supplementary Fig. S1f-h.

Human NQO1 is a dimer of identical subunits. Each subunit contains two domains: a catalytic domain and a C-terminal domain [25]. Each catalytic domain binds a flavin adenine dinucleotide (FAD) molecule, which forms a catalytic pocket with Trp105, Phe106, Gly149, Gly150, Tyr155, and His161 from one subunit and Tyr126, Tyr128, and Phe178 from the other subunit [26, 27]. A previous study has shown that the Leu103 participated in the stabilization of the FAD cofactor through the interaction with flavin rings [28]. The corresponding chemical structures of oroxylin A and SFII were shown in Fig. 2j. The binding poses of oroxylin A and SFII in NQO1 (PDB ID: 1D4A) were investigated via docking simulation studies. As shown in Fig. 2k, Trp105 formed π-π stacking with the benzene ring of oroxylin A. While the hydroxyl of SFII bind to the Leu103 and Gly149 of the catalytic domain with NQO1 via hydrogen bond (Fig. 2l).

In order to investigate the effect of oroxylin A and SFII on coagulation, the coagulation indexes (i.e., PT, APTT, and TT) were evaluated after C57BL/6 adult mice were orally administered with oroxylin A or SFII (6 mg/kg) for 24 h respectively (Fig. 2m). Dicoumarol was employed as a positive control and solvent olive oil as a negative control. It was found that PT, APTT, and TT were not significantly altered after the administration of oroxylin A or SFII to mice, while the same dose of dicoumarol could significantly elevate these indices (Fig. 2m). These results showed that SFII and oroxylin A would not affect the coagulation function in short term in vivo.

The inhibitory effect and affinity of oroxylin A and SFII with NQO1 recombinant protein have been explored previously, thus, we proceeded to test their inhibitory efficacy in L02 and HK-2. L02 cell line, originated from human normal hepatocytes, is an in vitro model of liver tissue to study pathological changes [29]. HK-2 cell line derived from primary human renal proximal tubular epithelial cells was used to estimate renal toxicity of AAI. Cells were treated with oroxylin A or SFII at 5 μM for 8 h before extracting protein. According to the activity assay, the inhibitory capability of SFII to NQO1 was significantly higher than oroxylin A in L02 (Fig. 2n). In HK-2, oroxylin A did not notably inhibit NQO1 activity compared with the control group. However, SFII still displayed a more efficient NQO1 inhibitory effect (Fig. 2n). As kidney is the well-known target organ for AAs-induced damage, SFII was selected as the most promising NQO1 inhibitor of the four candidates for the subsequent study.

## SFII could alleviate cell damage caused by AAI in L02 and HK-2

To explore the AAI-related damage in L02, we assessed cell proliferation and DNA damage under AAI treatment. First, we treated L02 with gradient doses of AAI (0, 5, 10, 20, 50, or 100 μM) for 48 h, and found that the anti-proliferative effects of AAI were gradually intensified (Fig. 3a). Additionally, DNA damage was examined by γ-H2AX expression, showing a considerable increase at the dose of 20 μM (Supplementary Fig. S3a). To observe the protective effect of SFII, cell proliferation was detected after L02 were treated with AAI (20 μM) or combined with SFII (5 or 10 μM) for 48 h. The inhibitory effect of AAI on cell proliferation was significantly relieved in AAI combined with SFII (5 or 10 μM) groups compared with cells treated with AAI alone (Fig. 3b). The protective effect of SFII on cells treated with a higher dose of AAI (50 μM) was similar (Supplementary Fig. S3b). In addition, SFII alone barely affected cell proliferation (Fig. 3b). In general, alanine aminotransferase (ALT) and aspartate aminotransferase (AST) are elevated when hepatocytes are damaged. Compared with the cells treated with AAI alone, the levels of ALT (Fig. 3c) and AST (Fig. 3d) in culture supernatant decreased when L02 was treated with SFII, showing a desirable protective effect. The effect of SFII was further confirmed in L02 with lentivirus containing the interfering sequence of NQO1 or negative control (shNQO1 or shNC) (Supplementary Fig. S2a). We examined NQO1 activity of shNQO1-L02 with or without SFII treatment (5 μM) for 8 h before extracting protein (Supplementary Fig. S2b). The result showed that NQO1 activity of shNQO1-L02 was lower than shNC-L02 probably due to NQO1 knockdown. Moreover, SFII treatment further reduced NQO1 activity of shNQO1-L02. As expected, SFII could further alleviate proliferation inhibition of AAI in L02-shNQO1 cells (Supplementary Fig. S2c). Additionally, cell damage was further reduced by SFII treatment in L02-shNQO1 cells (Supplementary Fig. S2d, e).

L02 was treated with AAI (20 μM, 50 μM) with or without SFII (5 or 10 μM) for 24 h. The percentage of apoptotic cells in SFII-treated groups was significantly decreased compared with the group treated with AAI alone (Fig. 3e). Similar to previous results, SFII could effectively reduce AAI-induced cell apoptosis in situ (Supplementary Fig. S3c). Whereas, SFII treatment alone did not affect the apoptosis of L02. To interrogate the mechanisms of how SFII treatment relieved AAI-induced apoptosis, our data suggested that SFII treatment could efficaciously decrease the expression of P53, cleaved caspase-3, and cleaved-PARP-1 as well as γ-H2AX (Fig. 3f). Besides, SFII could significantly downregulate mRNA levels of apoptotic-related genes, including *BAX, NOXA, PUMA*, and *BAK* (Fig. 3g). Furthermore, knockdown of NQO1 significantly decreased cell apoptosis (Supplementary Fig. S2f) and repressed apoptosis-related signaling (Supplementary Fig. S2g), while SFII could further reduce the damage caused by AAI in NQO1 knockdown cells. The above results indicated that SFII might exert a protective role against AAI-induced DNA damage.

Next, our study confirmed that HK-2 expressed a lower level of NQO1 compared with L02 (Supplementary Fig. S3d). The protective effect of SFII on AAI-induced damage in HK-2 was further explored. When treated with different doses of AAI, HK-2 cells exhibited better tolerance to AAI-induced proliferation inhibition (Fig. 4a). Thus, we selected the dose of 100 μM for AAI treatment in HK-2. AAI-induced inhibition of cell proliferation could be partially alleviated by SFII (Fig. 4b). Similarly, AAI could increase the expression of γ-H2AX in HK-2, particularly at the highest dose (100 μM) (Fig. 4c). While SFII could significantly decrease the expression of γ-H2AX and the expression of the downstream pro-apoptotic signaling (Fig. 4d). Furthermore, SFII also reduced the percentage of apoptotic cells in HK-2 in a dose-dependent manner (Fig. 4e). As shown in Supplementary Fig. S3e, the apoptotic cells in SFII-treated groups were significantly less than the group treated with AAI alone. Additionally, the expression of apoptosis-related genes such as *BAX, NOXA, PUMA*, and *BAK* was downregulated when HK-2 was treated with SFII (Fig. 4f). The above results indicated that SFII could effectively decrease AAI-induced DNA damage and cell apoptosis in L02 and HK-2.

## SFII effectively attenuated acute renal injury and fibrosis caused by AAI in vivo

The NQO1 activity was evaluated in kidney and liver tissues of mice, we found that SFII (30, 60 mg/kg) had a good inhibitory effect on NQO1 enzyme activity in vivo (Supplementary Fig. S4a). To assess the therapeutic potential of SFII in renal injury, we conducted AAI-induced renal injury model in adult mice. As in Fig. 5a, AAI (5 mg/kg) was injected to induce the acute renal injury model. In combined treatment group, mice were pretreated with SFII 12 h before AAI and SFII co-administration for 3 consecutive days. According to the previous study, when rats were administered with dicumarol at a dose of 20 mg/kg orally, it caused 60% of death within days [30]. Thus, in this study, dicumarol was not used as a positive intervention in vivo. Creatinine (CRE) is a common indicator to monitor acute renal injury. Our data suggested that AAI alone caused an elevation of blood CRE with a fold change of over 1.5, while it significantly declined in SFII

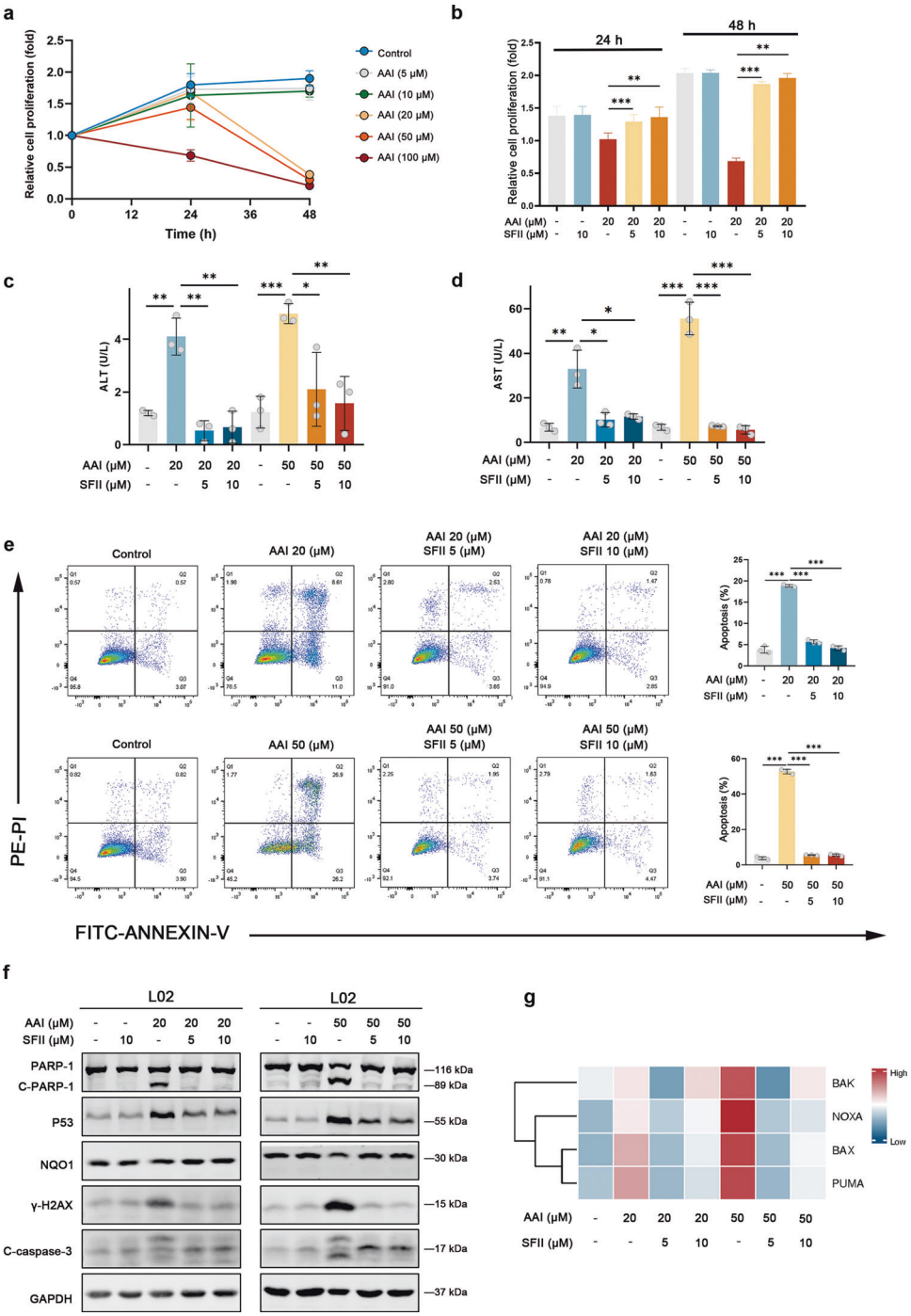


**Fig. 3 SFII inhibits AAI-induced DNA damage and apoptosis in L02. a** The CCK-8 analysis of cell proliferation in L02 treated with different concentrations of AAI. **b** SFII alleviated the inhibition of cell proliferation in L02 caused by AAI at the time of 24 h and 48 h. The **c** ALT and **d** AST levels in the culture medium of L02 after treatment with AAI (20 or 50 μM) with or without SFII (5 or 10 μM) for 24 h. **e** Flow cytometric analysis to detect the percentage of apoptosis in L02 treated with AAI (20 or 50 μM) with or without SFII (5 or 10 μM) for 24 h. Cell populations in Q2 (Annexin $V^+$, $PI^+$) and Q3 (Annexin $V^+$, $PI^-$) were considered as apoptotic cells. **f** Western blot analysis of L02 treated with either AAI (20 or 50 μM) or SFII or both for 24 h. **g** The qRT-PCR analysis of L02 was treated with either AAI (20 or 50 μM) or SFII or both for 24 h. C-caspase-3, cleaved caspase-3; C-PARP-1, cleaved-PARP-1; $^*P < 0.05$, $^{**}P < 0.01$, $^{***}P < 0.001$.

intervened groups (Fig. 5b). Although H&E showed no obvious histomorphological damage in kidney (Fig. 5c), the fibrosis area of SFII-treated groups was significantly limited than AAI alone group in a dose-dependent manner as indicated by Sirius red staining (Fig. 5d). TUNEL staining of kidney sections showed that SFII alleviated cell apoptosis, with no notable difference between groups of SFII treatment (Fig. 5e). Additionally, we found that the expressions of γ-H2AX, P53, cleaved-caspase-3, and cleaved-PARP-1 protein were downregulated in the groups with SFII treatment (Fig. 5f). These data indicated a protective role of SFII in AAI-induced acute renal injury via regulating apoptosis.

We further evaluated the role of SFII in AAI-induced renal fibrosis model. As in Fig. 5g, different from the acute kidney injury model, mice were sacrificed 14 days after the first dose of AAI. In

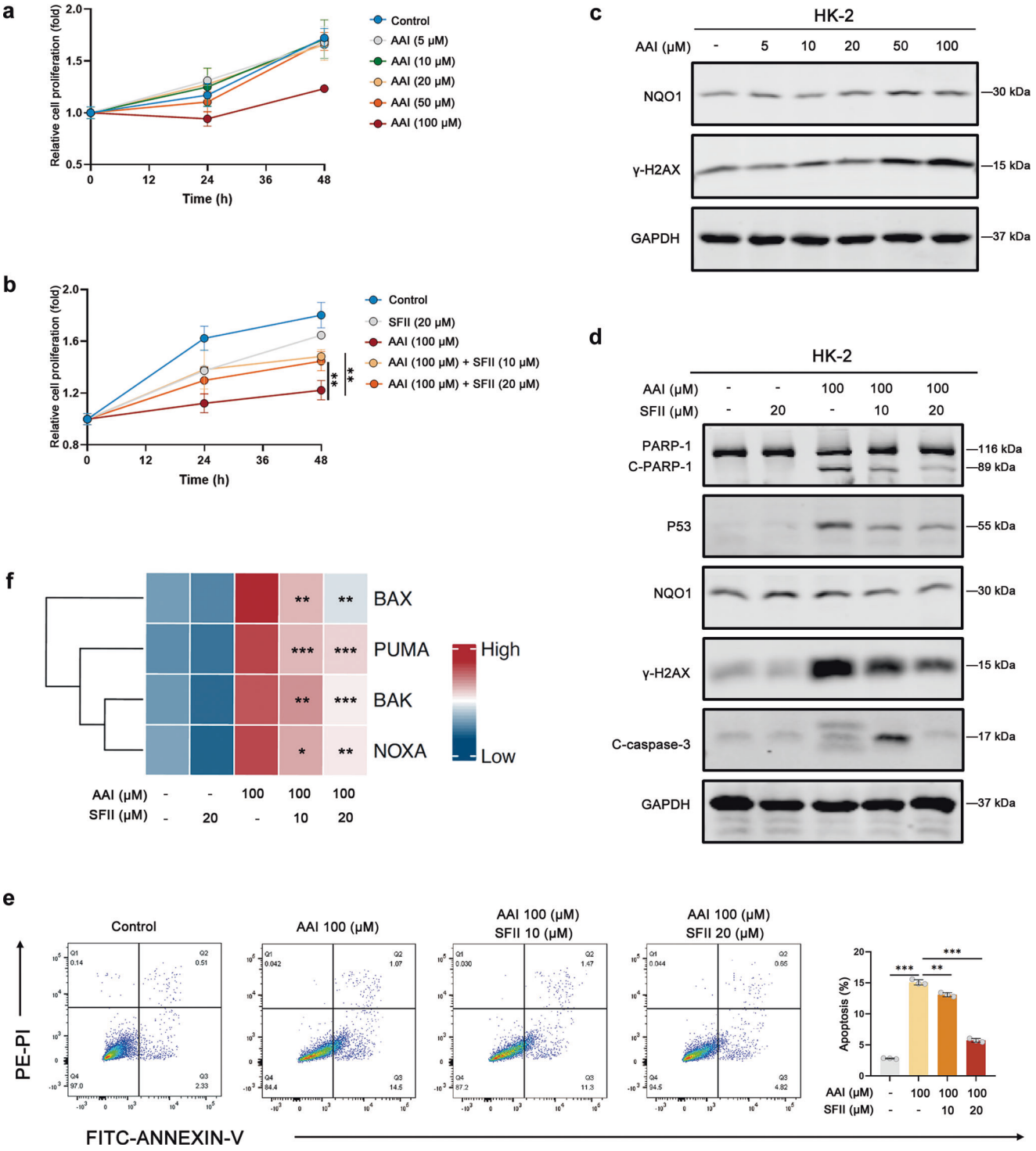


**Fig. 4 SFII inhibits AAI-induced DNA damage and apoptosis in HK-2. a** The CCK-8 analysis of cell proliferation in HK-2 treated with different concentrations of AAI. **b** The different concentrations of SFII alleviated the inhibition of cell proliferation in HK-2 caused by AAI for 48 h. **c** The DNA damage of HK-2 caused by a dose gradient of AAI was detected via Western blot. **d** Western blot analysis of HK-2 treated with either AAI or SFII or both for 24 h. **e** Flow cytometric analysis to detect the percentage of apoptosis in HK-2 treated with AAI with or without SFII (10 or 20 μM) for 24 h. **f** The qRT-PCR analysis of HK-2 treated with either AAI or SFII or both for 24 h. Asterisks indicate the significant difference between AAI group and the SFII and AAI combined treatment group. *$P < 0.05$, **$P < 0.01$, ***$P < 0.001$.

this model, blood urea (UREA) was also examined to monitor the biological function of kidney. Compared with the AAI group, the levels of blood CRE and UREA were significantly decreased in mice receiving SFII treatment in a dose-dependent manner (Fig. 5h). As expected, the H&E and Sirius red staining showed that AAI induced significant renal interstitial fibrosis, whereas SFII effectively relieved renal tubular atrophy and interstitial fibrosis (Fig. 5i and Supplementary Fig. S4b). In conclusion, these models demonstrated that SFII could effectively alleviate renal injury caused by AAI in adult mice.

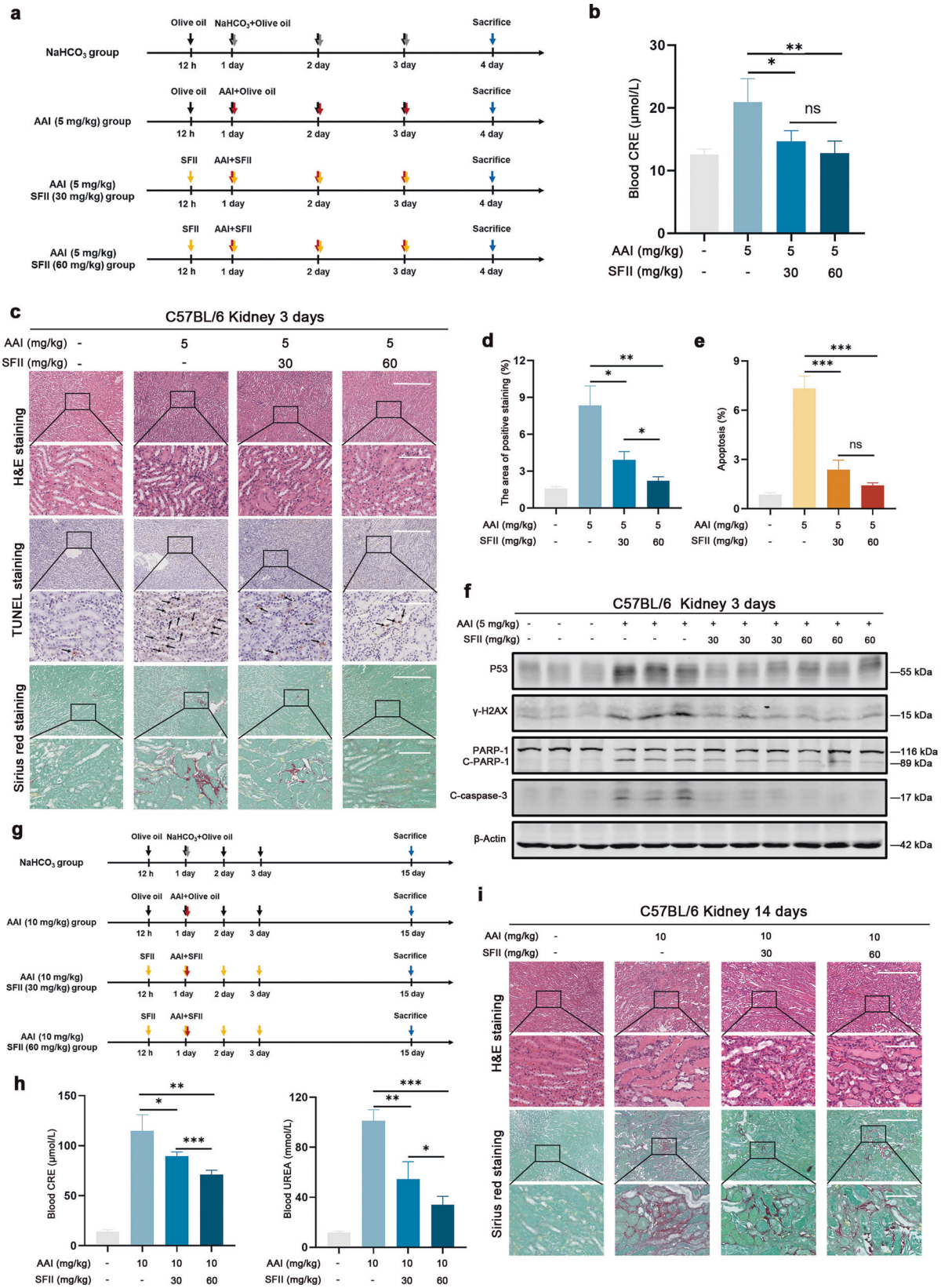


SFII could suppress AAI-induced liver injury and hepatocarcinogenesis in vivo

Previous study found that the adult mouse liver was not the principal target of AAI-related toxicity. ALT and AST levels were barely elevated after 4 months of consecutive AAI treatment [6]. In this study, when adult and infant mice (at the age of 14 days) were injected with PBS (as a negative control), diethylnitrosamine (DEN, as a positive control) or AAI (20 mg/kg) and sacrificed after 24 h.

**Fig. 5 SFII showed an inhibitory effect on AAI induced acute injury and fibrosis in the kidney of adult mice. a** Schematic representation of the three-days treatment in different groups of adult mice. Mice were intraperitoneally (*i.p.*) injection with $NaHCO_3$ (gray arrow) or AAI (red arrow, 5 mg/kg) for three consecutive days as the $NaHCO_3$ group or AAI group. The SFII treatment group was administered (oral) with SFII (orange arrow) 12 h before injecting AAI and at the time of injection. **b** The levels of blood CRE in different groups after three-day treatment. **c** Representative images of H&E staining (scale bars, 500 or 100 μm), TUNEL staining (scale bars, 500 or 100 μm), and Sirius red staining (scale bars, 500 or 100 μm) of kidney samples in different treatment groups. The black arrows point to apoptosis cells in the kidney. **d** The staining area of kidney fibrosis was calculated. **e** The percentage of renal cell apoptosis was calculated. **f** Western blot analysis to evaluate the AAI-induced kidney injury in adult mice treated with or without SFII. **g** Design of SFII administration in renal fibrosis model of adult mice. Mice were injected (*i.p.*) with a single dose of $NaHCO_3$ (gray arrow) or AAI (red arrow, 10 mg/kg) as the $NaHCO_3$ group or AAI group. The SFII treatment group received SFII (orange arrow) 12 h before AAI administration and three consecutive days after a single dose of AAI. Mice were sacrificed 14 days after a single dose of $NaHCO_3$ or AAI. **h** The level of blood CRE and UREA in different treatment groups. **i** Representative images of H&E staining (scale bars, 500 or 100 μm) and Sirius red staining (scale bars, 500 or 100 μm) of kidney samples in different treatment groups. $^*P < 0.05$, $^{**}P < 0.01$, $^{***}P < 0.001$.

AAI scarcely caused DNA damage in the liver of adult mice, while it induced an upregulation of γ-H2AX in the liver of infant mice (Supplementary Fig. S4c). Therefore, we focused on whether SFII could alleviate the injury induced by AAI in infant mice.

As shown in Fig. 6a, in SFII intervention group, infant mice were pretreated with SFII 12 h before a single injection of AAI. Our results showed that AAI did induce DNA damage and apoptosis in the liver and kidney of infant mice. The expression of DNA damage and apoptosis-related proteins were significantly decreased when mice were pretreated with SFII (Fig. 6b and Supplementary Fig. S4d). Similarly, we found that the proportion of apoptotic cells in SFII pre-treated group was also decreased in the liver, compared with the AAI treatment alone group (Fig. 6c, d). No obvious liver fibrosis was observed in each group (Fig. 6e). Whereas, SFII reduced cell apoptosis as well as interstitial fibrosis caused by AAI in kidney (Supplementary Fig. S4e).

Our preceding study demonstrated that AAI could induce liver tumors when objected to infant mice [6]. To further explore whether SFII could directly suppress genotoxic of AAI, infant mice were pretreated with SFII in AAI-induced liver cancer model and then sacrificed 16 weeks after AAI administration (Fig. 6f). Liver tumors were formed in each group except for the $NaHCO_3$ group as demonstrated by Ki-67 and alpha-fetoprotein (AFP) staining (Fig. 6g). Mice administered with SFII exhibited a significant decrease in the number of tumors per liver dose-independently (Fig. 6h). Furthermore, kidney fibrosis was notably relieved in mice treated with SFII (Supplementary Fig. S4f). Taken together, these data indicated that SFII could effectively alleviate AAI-induced hepatorenal injury and hepatocarcinogenesis in infant mice.

## DISCUSSION

Aristolochic acids (AAs) are a class of natural compounds that widely exist in medicinal herbs of Aristolochiaceae [31]. The safe use of AAs has been seriously hindered due to AAs-induced organ damage [32]. Screening and identifying compounds that can alleviate the toxicity of AAs is an effective strategy to reduce the adverse reaction of the involved Chinese herbal medicine. Therefore, we aimed to find natural compounds to alleviate the toxicity of AAs.

In this study, we constructed NQO1 biochromatography stationary phase to screen the potential components from the extract of *Scutellaria baicalensis*, which could bind to NQO1 protein. Based on the data obtained from the comprehensive 2D NQO1 biochromatography system, four candidates derived from the extract of *Scutellaria baicalensis* were further evaluated for SPR and NQO1 activity inhibition test. The results showed that SFII had a good affinity with NQO1 protein and an excellent effect on NQO1 inhibition. Notably, SFII did not directly repress the expression of NQO1, but reduce DNA damage by inhibiting the activity of NQO1. Subsequently, the biological effect of SFII was further identified by inhibiting NQO1 activity in cells. Our data showed that SFII could effectively alleviate the inhibitory effect of AAI on cell proliferation and reduce cell apoptosis.

Although oroxylin A displayed good affinity and inhibition effect on the human NQO1 recombinant protein, the inhibition of NQO1 activity by oroxylin A was not as desirable as SFII in cells (Fig. 2n). The actual inhibitory effect of an agent to the target in cells can not be simulated completely by pure protein affinity experiment since the microenvironment is much more complicated in cells. In addition, oroxylin A, as a multi target inhibitor, has many binding targets, such as L-plastin (LPL) [33], transketolase (TKT) [34], angiotensin converting enzyme II (ACE2) [35], cyclooxygenase 2 (Cox-2), inducible nitric oxide synthase (iNOS), glycogen synthase kinase-3β (GSK-3β) [36], etc. These targets might competitively bind oroxylin A with NQO1, which may impair the binding of oroxylin A to NQO1.

According to the literature, the kidney is the principal target organ of AAI, with the damage manifested as cell apoptosis and renal fibrosis [37–39]. Renal fibrosis is a pathological change of the kidney caused by various factors, including injury and inflammation [40]. The early event of renal injury is tubular apoptosis, which releases cytokines and chemokines, leading to inflammatory response and interstitial fibrosis [41]. In the adult mouse model, the fibrosis and cell apoptosis of renal in the SFII treatment group was significantly reduced compared with the AAI alone group (Fig. 5c, i). Therefore, we speculated that SFII could inhibit interstitial fibrosis by repressing the apoptosis of renal cells caused by AAI.

The liver is the major detoxifying organ, and the enzyme system of the liver plays a key role in the biotransformation of drugs and carcinogens [42]. Adult mice have a full enzyme system in the liver; however, the xenobiotic-metabolizing enzymes, such as cytochrome P450, are rarely expressed in infant mice [43, 44]. In the infant mouse model, SFII could effectively relieve AAI-induced DNA damage and apoptosis of the liver and kidney (Fig. 6b-e and Supplementary Fig. S4d, e) and suppress the tumorigenicity of AAI (Fig. 6g, h). The hepatocytes of infant mice are at the rapid proliferative phase, which is conducive to the fixation of gene mutation caused by DNA damage, laying the seeds for liver cancer [45, 46]. We hypothesized that DNA damage caused by AAI was reduced by SFII, which then prevented the accumulation of DNA mutations, and in turn repressed tumorigenesis.

The level of biological activation of AAI was associated with NQO1 activity [8, 47]. NQO1 functions through the ping-pong mechanism, in which NAD(P)H first enters the active site and then transfers hydride into FAD. Then, the oxidized $NAD(P)^+$ leaves the active site, and the substrate is reduced via entering the site [48]. Dicoumarol, the typical NQO1 inhibitor competes with NAD(P)H for binding to NQO1, thereby represses the function of FAD [49]. However, the structure of dicoumarol is similar to vitamin K, which competitively combines with vitamin K epoxide reductase, inhibiting the vitamin K-dependent γ-carboxylation of glutamate residues [11, 50, 51]. It has been demonstrated that dicoumarol could prolong PT and APTT in various mammal species [30, 52]. In our study, when adult mice were administered with SFII for 24 h, it barely prolonged PT, APTT, or TT compared with the control group (Fig. 2m). The proliferation and apoptosis of cells were not

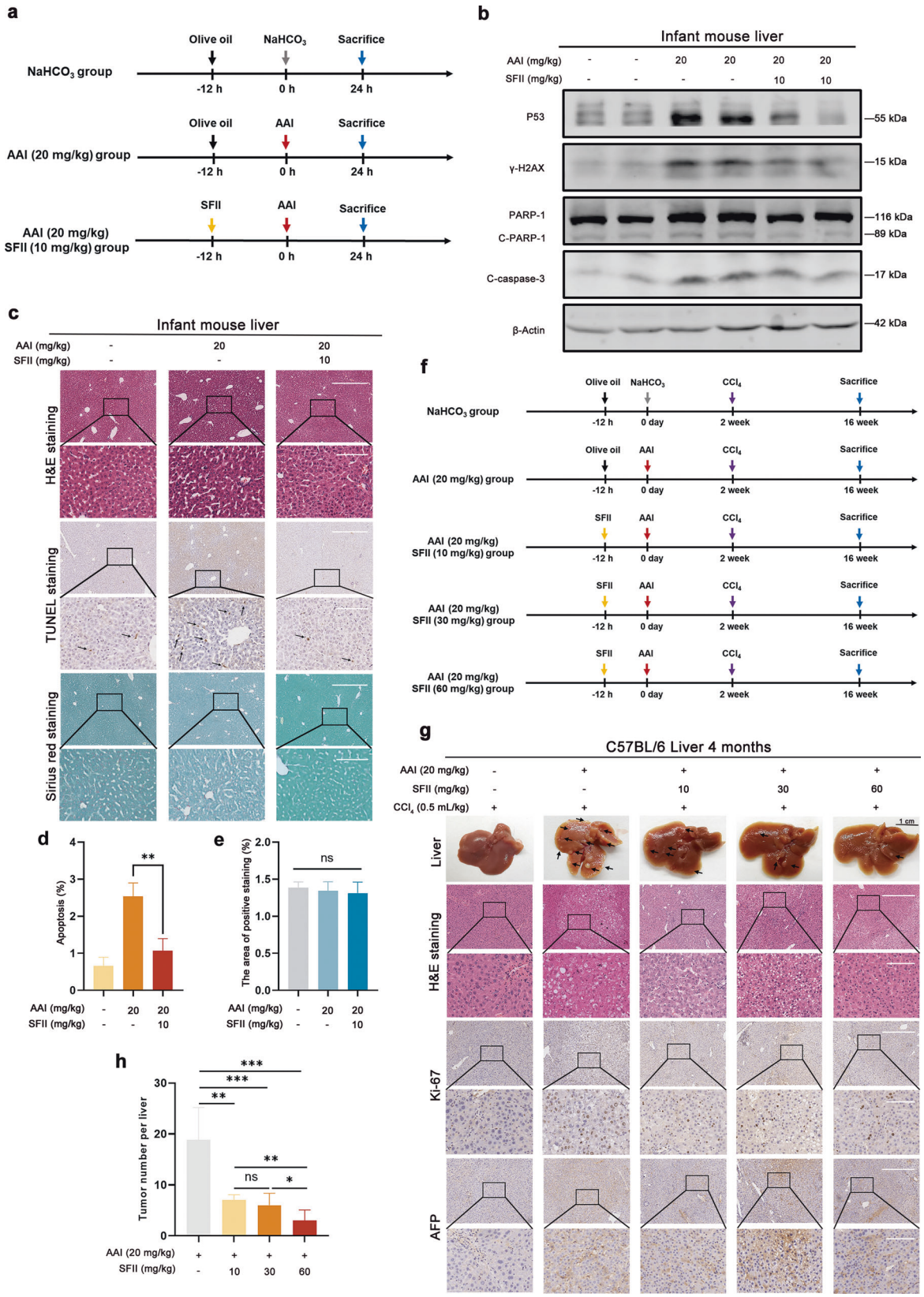


affected by SFII alone at the therapeutic dose of 5 μM in vitro. Furthermore, in adult mice renal fibrosis model, AAI caused intensive weight loss of mice as previous report indicated [6]. There was no significant change of the body weight in mice pretreated with SFII. With a similar inhibitory effect on NQO1 and fewer side effects than dicoumarol, SFII might serve as a potential candidate drug for clinical practice. Admittedly, more comprehensive study is needed to evaluate the safety of SFII in vivo.

**Fig. 6 The protective and anticancer effect of SFII in the liver of infant mice. a** Schematic representation of the short-term observation of AAI and SFII administration in infant mice. At 14 days of birth, mice were injected with $NaHCO_3$ (gray arrow) or AAI (red arrow). The $NaHCO_3$ group or AAI group were also pretreated with olive oil (black arrow, *i.p.*) 12 h before $NaHCO_3$ or AAI administration. In the SFII treatment group, the mice were injected with SFII (orange arrow) 12 h before injection of AAI. **b** Western blot to detect the AAI-induced liver injury in infant mice treated with or without SFII. **c** Representative images of H&E staining (scale bars, 500 or 100 μm), TUNEL staining (scale bars, 500 or 100 μm), and Sirius red staining (scale bars, 500 or 100 μm) of the liver samples in infant mice treated with or without SFII. The black arrows point to apoptosis cells in the liver. **d** The percentage of hepatocyte apoptosis was calculated. **e** The staining area of liver fibrosis was calculated. **f** Schematic representation of the regimens of AAI and SFII administration in liver cancer model. At 14 days of birth, mice were injected with a single dose of $NaHCO_3$ (gray arrow) or AAI (red arrow). The $NaHCO_3$ group or AAI group were pretreated with oral olive oil (black arrow) 12 h before $NaHCO_3$ or AAI administration. The mice were pretreated with oral SFII (orange arrow) 12 h before a single injection of AAI (red arrow) in the SFII treatment group. $CCl_4$ was administered (*i.p.*) 2 weeks after the first shot of AAI for 14 weeks (once per week). **g** The representative pictures of gross (scale bars, 1 cm), H&E staining (scale bars, 500 or 100 μm), Ki-67 staining (scale bars, 500 or 100 μm), and AFP staining (scale bars, 500 or 100 μm) of the liver samples of mice after 16 weeks of AAI administration were presented. The black arrows point to the tumor in the liver. **h** The tumor number per liver in different treatment groups was calculated. $^{*}P < 0.05$, $^{**}P < 0.01$, $^{***}P < 0.001$.

It was reported that dicoumarol could promote the degradation of hepatitis B virus (HBV) protein HBx and then significantly inhibit the transcription of HBV covalently closed circular DNA (cccDNA) [53]. In addition, knockdown of NQO1 in HCC cells significantly reduced tumor volume in mouse xenograft model [54]. In our study, SFII, as an NQO1 inhibitor, also effectively repressed the carcinogenesis in the liver. Therefore, as an NQO1 inhibitor, the indications of SFII might be extended to NQO1-mediated diseases, including but not limited to hepatorenal injury caused by AAs.

## CONCLUSION

In the present study, the comprehensive 2D biochromatography system is used to screen natural inhibitors of NQO1 from *Scutellaria baicalensis*. SFII showed high affinity and inhibition effect on NQO1. Our data demonstrated that SFII could alleviate AAI-induced DNA damage and hepatorenal toxicity in vivo and in vitro by inhibiting NQO1 activity without showing obvious side effect. Therefore, SFII could protect hepatorenal toxicity induced by AAI via inhibiting NQO1 activity, showing a good potential for further clinical application.

## ACKNOWLEDGEMENTS

We would like to thank the support from the Shanghai Key Laboratory of Hepatobiliary Tumor Biology and Military Key Laboratory and Targeting Therapy of Liver Cancer, Second Military Medical University, Shanghai, China. We thank Ms. Lu Chen, Ms. Dan Cao, Ms. Lin-na Guo, and Ms. Shan-hua Tang from International Cooperation Laboratory on Signal Transduction for their technical support. This work was supported by the Ministry of Science and Technology Key Program for "Significant New Drugs Development" (2018ZX09101002, 2018ZX09101002-001-001, 2018ZX09101002-001-002). Funding for this project was also provided by the National Natural Science Foundation of China (81830054, 91859205, 82072600, 81973291, and 82122066). The plan of Shanghai Municipal Health Commission (2022XD036) also provided funding to conduct this project.

## AUTHOR CONTRIBUTIONS

YPD, WW, and HYW designed the study. YPD, SZC, and HSH developed the methodology. YPD, ZRS, YQG, and YZ acquired data. SZC, YPD, HSH, and FF analyzed and interpreted data. YPD, SZC, and LXJ wrote and reviewed the manuscript. ZCF, HSH, and CC provided technical and material support. XFC, WW, and HYW supervised the study.

## ADDITIONAL INFORMATION

**Supplementary information** The online version contains supplementary material available at https://doi.org/10.1038/s41401-023-01052-3.

**Competing interests:** The authors declare no competing interests.

## REFERENCES

1. Yang HY, Chen PC, Wang JD. Chinese herbs containing aristolochic acid associated with renal failure and urothelial carcinoma: a review from epidemiologic observations to causal inference. Biomed Res Int. 2014;2014:569325.
2. Zhang H, Liu R, An Z, Li H, Zhang R, Zhou F. Aristolactam-type alkaloids and aristolochic acids from *Aristolochia moupinensis* and *Aristolochia cathcartii*. Biochem Syst Ecol. 2016;65:198–201.
3. Sato N, Takahashi D, Chen SM, Tsuchiya R, Mukoyama T, Yamagata S, et al. Acute nephrotoxicity of aristolochic acids in mice. J Pharm Pharmacol. 2004;56:221–9.
4. Vanhaelen M, Vanhaelen FR, But P, Vanherweghem JL. Identification of aristolochic acid in Chinese herbs. Lancet. 1994;343:174.
5. Schmeiser HH, Bieler CA, Wiessler M, Ypersele C, Cosyns JP. Detection of DNA adducts formed by aristolochic acid in renal tissue from patients with Chinese herbs nephropathy. Cancer Res. 1996;56:2025–8.
6. Chen S, Dong Y, Qi X, Cao Q, Luo T, Bai Z, et al. Aristolochic acids exposure was not the main cause of liver tumorigenesis in adulthood. Acta Pharm Sin B. 2021;12:2252–67.
7. Stiborová M, Arlt VM. DNA adducts formed by aristolochic acid are unique biomarkers of exposure and explain the initiation phase of upper urothelial cancer. Int J Mol Sci. 2017;18:2144.
8. Stiborová M, Frei E, Sopko B, Sopková K, Marková V, Lanková M, et al. Human cytosolic enzymes involved in the metabolic activation of carcinogenic aristolochic acid: evidence for reductive activation by human NAD(P)H:quinone oxidoreductase. Carcinogenesis. 2003;24:1695–703.
9. Parkinson EI, Bair JS, Cismesia M, Hergenrother PJ. Efficient NQO1 substrates are potent and selective anticancer agents. ACS Chem Biol. 2013;8:2173–83.
10. Danson S, Ward TH, Butler J, Ranson M. DT-diaphorase: a target for new anticancer drugs. Cancer Treat Rev. 2004;30:437–49.
11. Timson DJ. Dicoumarol: a drug which hits at least two very different targets in vitamin K metabolism. Curr Drug Targets. 2017;18:500–10.
12. Betancor FI, Timson DJ, Salido E, Pey AL. Natural (and unnatural) small molecules as pharmacological chaperones and inhibitors in cancer. Handb Exp Pharmacol. 2018;245:155–90.
13. Cheng CS, Chen J, Tan HY, Wang N, Chen Z, Feng Y. *Scutellaria baicalensis* and cancer treatment: recent progress and perspectives in biomedical and clinical studies. Am J Chin Med. 2018;46:25–54.
14. Zhang G, Li C, Niu Y, Yu Q, Chen Y, Liu E. Osteoprotective effect of radix scutellariae in female hindlimb-suspended sprague-dawley rats and the osteogenic differentiation effect of its major constituent. Molecules. 2017;22:1044.
15. Zhao T, Tang H. *Scutellaria baicalensis Georgi*. (Lamiaceae): a review of its traditional uses, botany, phytochemistry, pharmacology and toxicology. J Pharm Pharmacol. 2019;71:1353–69.
16. Huang TH, Wu TH, Guo YH, Li TL, Chan YL, Wu CJ. The concurrent treatment of *Scutellaria baicalensis Georgi* enhances the therapeutic efficacy of cisplatin but also attenuates chemotherapy-induced cachexia and acute kidney injury. J Ethnopharmacol. 2019;243:112075.
17. Xu J, Li S, Jiang L, Gao X, Liu W, Zhu X, et al. Baicalin protects against zearalenone-induced chicks liver and kidney injury by inhibiting expression of oxidative stress, inflammatory cytokines and caspase signaling pathway. Int Immunopharmacol. 2021;100:108097.
18. He Q, Sun X, Zhang M, Chu L. Protective effect of baicalin against arsenic trioxide-induced acute hepatic injury in mice through JAK2/STAT3 signaling pathway. Int J Immunopathol Pharmacol. 2022;36:https://doi.org/10.1177/20587384211073397.
19. Wang X, Chang X, Zhan H, Zhang Q, Li C, Gao Q, et al. Curcumin and baicalin ameliorate ethanol-induced liver oxidative damage via the Nrf2/HO-1 pathway. J Food Biochem. 2020;44:e13425.
20. Chen C, Yang FQ, Zuo HL, Song YL, Xia ZN, Xiao W. Applications of biochromatography in the screening of bioactive natural products. J Chromatogr Sci. 2013;51:780–90.
21. Chen X, Wu Y, Chen C, Gu Y, Zhu C, Wang S, et al. Identifying potential anti-COVID-19 pharmacological components of traditional Chinese medicine

Lianhuaqingwen capsule based on human exposure and ACE2 biochromatography screening. Acta Pharm Sin B 2021;11:222–36.
22. Chen X, Cao Y, Zhang H, Zhu Z, Liu M, Liu H, et al. Comparative normal/failing rat myocardium cell membrane chromatographic analysis system for screening specific components that counteract doxorubicin-induced heart failure from *Acontium carmichaeli*. Anal Chem. 2014;86:4748–57.
23. Chen X, Cao Y, Lv D, Zhu Z, Zhang J, Chai Y. Comprehensive two-dimensional HepG2/cell membrane chromatography/monolithic column/time-of-flight mass spectrometry system for screening anti-tumor components from herbal medicines. J Chromatogr A. 2012;1242:67–74.
24. Olaru A, Bala C, Jaffrezic RN, Aboul EHY. Surface plasmon resonance (SPR) biosensors in pharmaceutical analysis. Crit Rev Anal Chem. 2015;45:97–105.
25. Faig M, Bianchet MA, Talalay P, Chen S, Winski S, Ross D, et al. Structures of recombinant human and mouse NAD(P)H:quinone oxidoreductases: species comparison and structural changes with substrate binding and release. Proc Natl Acad Sci USA. 2000;97:3177–82.
26. Pidugu LS, Mbimba JC, Ahmad M, Pozharski E, Sausville EA, Emadi A, et al. A direct interaction between NQO1 and a chemotherapeutic dimeric naphthoquinone. BMC Struct Biol. 2016;16:1.
27. Nolan KA, Doncaster JR, Dunstan MS, Scott KA, Frenkel AD, Siegel D, et al. Synthesis and biological evaluation of coumarin-based inhibitors of NAD(P)H: quinone oxidoreductase-1 (NQO1). J Med Chem. 2009;52: 7142–56.
28. Skelly JV, Sanderson MR, Suter DA, Baumann U, Read MA, Gregory DS, et al. Crystal structure of human DT-diaphorase: a model for interaction with the cytotoxic prodrug 5-(aziridin-1-yl)-2,4-dinitrobenzamide (CB1954). J Med Chem. 1999;42:4325–30.
29. Cheng B, Zheng Y, Guo X, Wang Y, Liu C. Hepatitis B viral X protein alters the biological features and expressions of DNA repair enzymes in LO2 cells. Liver Int. 2010;30:319–26.
30. Chandrasekhar N, Hickie RA, Millar GJ. The effect of dicumarol on prothrombin time in rats and its relation to vitamin k content of liver. Can J Physiol Pharmacol. 1965;43:639.
31. Veale EL, Mathie A. Aristolochic acid, a plant extract used in the treatment of pain and linked to Balkan endemic nephropathy, is a regulator of K2P channels. Br J Pharmacol. 2016;173:1639–52.
32. Jadot I, Declèves AE, Nortier J, Caron N. An integrated view of aristolochic acid nephropathy: update of the literature. Int J Mol Sci. 2017;18:297.
33. Li X, Wang L. Targeting actin-bundling protein L-plastin as an anabolic therapy for bone loss. Sci Adv. 2020;6:eabb7135.
34. Jia D, Liu C, Zhu Z, Cao Y, Wen W, Hong Z, et al. Novel transketolase inhibitor oroxylin A suppresses the non-oxidative pentose phosphate pathway and hepatocellular carcinoma tumour growth in mice and patient-derived organoids. Clin Transl Med. 2022;12:e1095.
35. Gao J, Ding Y, Wang Y, Liang P, Zhang L, Liu R. Oroxylin A is a severe acute respiratory syndrome coronavirus 2-spiked pseudotyped virus blocker obtained from *Radix Scutellariae* using angiotensin-converting enzyme II/cell membrane chromatography. Phytother Res. 2021;35:3194–204.
36. Sajeev A, Hegde M. Oroxylin A: a promising flavonoid for prevention and treatment of chronic diseases. Biomolecules. 2022;12:1185.
37. Bunel V, Antoine MH, Nortier J, Duez P, Stévigny C. In vitro effects of panax ginseng in aristolochic acid-mediated renal tubulotoxicity: apoptosis versus regeneration. Planta Med. 2015;81:363–72.
38. Huang L, Scarpellini A, Funck M, Verderio EA, Johnson TS. Development of a chronic kidney disease model in C57BL/6 mice with relevance to human pathology. Nephron Extra. 2013;3:12–29.
39. Chen F, Gao Q, Wei A, Chen X, Shi Y, Wang H. Histone deacetylase 3 aberration inhibits Klotho transcription and promotes renal fibrosis. Cell Death Differ. 2021;28:1001–12.
40. Li S, Xiao X, Han L, Wang Y, Luo G. Renoprotective effect of Zhenwu decoction against renal fibrosis by regulation of oxidative damage and energy metabolism disorder. Sci Rep. 2018;8:14627.
41. Mizuguchi Y, Chen J, Seshan SV, Poppas DP, Szeto HH, Felsen D. A novel cell-permeable antioxidant peptide decreases renal tubular apoptosis and damage in unilateral ureteral obstruction. Am J Physiol Ren Physiol. 2008;295:1545–53.
42. Nebert DW, Dalton TP. The role of cytochrome P450 enzymes in endogenous signalling pathways and environmental carcinogenesis. Nat Rev Cancer. 2006;6:947–60.
43. Hart SN, Cui Y, Klaassen CD, Zhong XB. Three patterns of cytochrome P450 gene expression during liver maturation in mice. Drug Metab Dispos. 2009;37:116–21.
44. Peng L, Cui JY, Yoo B, Gunewardena SS, Lu H, Klaassen CD, et al. RNA-sequencing quantification of hepatic ontogeny of phase-I enzymes in mice. Drug Metab Dispos. 2013;41:2175–86.
45. Hanigan MH, Kemp CJ, Ginsler JJ, Drinkwater NR. Rapid growth of preneoplastic lesions in hepatocarcinogen-sensitive C3H/HeJ male mice relative to C57BL/6J male mice. Carcinogenesis. 1988;9:885–90.
46. Vesselinovitch SD, Mihailovich N. Kinetics of diethylnitrosamine hepatocarcinogenesis in the infant mouse. Cancer Res. 1983;43:4253–9.
47. Levova K, Moserova M, Nebert DW, Phillips DH, Frei E, Schmeiser HH, et al. NAD(P)H:quinone oxidoreductase expression in Cyp1a-knockout and CYP1A-humanized mouse lines and its effect on bioactivation of the carcinogen aristolochic acid I. Toxicol Appl Pharmacol. 2012;265:360–7.
48. Hosoda S, Nakamura W, Hayashi K. Properties and reaction mechanism of DT diaphorase from rat liver. J Biol Chem. 1974;249:6416–23.
49. Zhang K, Chen D, Ma K, Wu X, Hao H. NAD(P)H:quinone oxidoreductase 1 (NQO1) as a therapeutic and diagnostic target in cancer. J Med Chem. 2018;61:6983–7003.
50. Macmillan RL. Observation on the mechanism of action of dicoumarol. Science. 1948;108:416–7.
51. Nelsestuen GL, Suttie JW. The purification and properties of an abnormal prothrombin protein produced by dicumarol-treated cows. A comparison to normal prothrombin. J Biol Chem. 1972;247:8176–82.
52. Runciman DJ, Lee AM, Reed KF, Walsh JR. Dicoumarol toxicity in cattle associated with ingestion of silage containing sweet vernal grass (anthoxanthum odoratum). Aust Vet J. 2002;80:28–32.
53. Cheng ST, Hu JL, Ren JH, Yu HB, Zhong S, Wai Wong VK, et al. Dicoumarol, an NQO1 inhibitor, blocks cccDNA transcription by promoting degradation of HBx. J Hepatol. 2021;74:522–34.
54. Yang Y, Zheng J, Wang M. NQO1 promotes an aggressive phenotype in hepatocellular carcinoma via amplifying ERK-NRF2 signaling. Cancer Sci. 2021;112:641–54.